Large eddy simulation of a wind turbine airfoil at high angle of attack

By P. Venugopal†, L. Cheung†, G. Jothiprasad† AND S. K. Lele

Large Eddy Simulation (LES) is used to study the airflow characteristics of the DU96 airfoil at a near-stall angle of attack and a chord-based Reynolds number of 1.5 million. Results from the LES are compared to experimental data and to panel method predictions. An initial LES conducted with poor spanwise resolution failed to predict suction side separation found in experiments. Evolution of the suction side boundary layer and skin friction distribution as well as initial results from an LES with improved spanwise resolution are presented.

1. Introduction

The ability to design low-noise wind turbine blades will allow for larger, lightweight blades that can capture more power from existing wind resources. Given that blade noise scales as fifth power of tip-speed, a 1 dBA quieter design enables a 2-3% increase in annual energy yield from the same installation with a larger rotor.

A major portion of the radiated noise for wind turbine blades is airfoil self-noise, which is also a function of angle of attack (Brooks *et al.* 1989). Because of the environment in which these blades operate, they often experience rapid changes in angle of attack. A sudden change in wind speed or wind direction can alter the local angle of attack. In the case of downwind turbines, the presence of the tower wake alters the angle of attack as the rotor blades move in and out of the wake. In a wind farm, wakes from upstream turbines can affect the angle of attack on downstream turbines. Hence, to design highly-efficient, low-noise wind turbines, it is imperative to fully quantify the sensitivity of airfoil self-noise to angle-of-attack.

At different angles of attack, different self-noise mechanisms become important. At low angles of attack, the major source of airfoil self-noise is trailing edge noise, which is the noise generated through the scattering of turbulent boundary layer fluctuations by the trailing edge. At moderate to high angles of attack, there could be flow separation on the suction side of the airfoil and the shed vorticity can generate trailing edge noise (Brooks *et al.* 1989). At very high angles of attack, there is massive suction side separation and low frequency noise is radiated from the chord as a whole (Brooks *et al.* 1989). At GE Global Research, LES has been used to study the noise generated by a representative wind turbine airfoil at a moderate angle of attack (Wolf *et al.* 2012). The objective of this report is to extend that study to a near-stall angle of attack case, with the ultimate aim of understanding variations in far-field noise signature with respect to angle of attack.

In recent years, there have been several articles in the open literature on the use of LES to compute airfoil self-noise, primarily trailing edge noise. Different airfoil shapes have been studied, mainly at low to moderate angles of attack. These include the studies

† General Electric Global Research Center, Niskayuna, NY, 12309

by Wang & Moin (2000) for a flat strut with an asymmetrically beveled trailing edge at 0 degree angle of attack, Manoha *et al.* (2002) for a NACA 0012 airfoil at 5 degree angle of attack, Oberai *et al.* (2002) for an Eppler 387 airfoil, Wang *et al.* (2004) for a controlled diffusion airfoil employed in an industrial fan at 8 degree angle of attack, Winkler *et al.* (2009*b*,*a*) for a NACA 6512-63 airfoil at 0 degree angle of attack and Gloerfet & Garrec (2009) for a NACA 0012 airfoil at 2.5 degree angle of attack. Lastly, Wolf & Lele (2011) studied the generation and propagation of broadband and tonal noise for different flow conditions over a NACA 0012 airfoil. They also studied the hydrodynamic and acoustic scaling of noise.

However, the impact of turbulent quantities on self-noise generation by modern, high-lift, cambered wind turbine airfoils at high angles of attack is yet to be addressed. To our knowledge, the only study that has used LES to predict trailing edge noise at high angles of attack is by Christophe *et al.* (2009). They used incompressible LES to predict the far field noise of a controlled diffusion airfoil used in automotive fans at 8 and 15 degree angles of attack. These simulations were performed at a moderate chord-based Reynolds number of $160,000$ and the results compared to experiments of Moreau & Roger (2005). Their simulations showed that LES predicted the measured trends for the wall-pressure spectra near the trailing edge, although it over-predicted the energy at low frequencies. Far field noise predictions, using Amiet's theory, also showed similar behavior.

The present investigation involves the simulation of airflow around a representative wind turbine airfoil with the ultimate aim of predicting the broadband noise that arises from the airfoil. This airfoil has a sharper trailing edge than those previously studied. The flow is simulated at a larger chord-based Reynolds number of 1.5 million and at a near stall angle of attack.

2. Simulation details

The representative wind turbine blade section chosen for this study is the DU96 airfoil. Virginia Tech. undertook an extensive experimental study of the aerodynamics and acoustics of this airfoil (Devenport *et al.* 2008) and provides a rich database against which to compare the computational results. The angle of attack chosen for this study is 10.3°, which the experiment indicates is close to the stall point of this airfoil. The chosen Reynolds number based on free-stream conditions and airfoil chord is 1.5 million. This was to be consistent with an earlier LES that was done for the same airfoil at a moderate angle of attack of 6.2° (Wolf *et al.* 2012).

The fluid is assumed to be incompressible as the free-stream Mach number is low ($M = 0.067$). The incompressible Navier-Stokes equations are solved using an incompressible version of charLES. This code is capable of handling unstructured grids and computes the flux at each control volume face using a blend of non-dissipative central flux and dissipative upwind flux (Khalighi *et al.* 2011). To minimize the numerical dissipation introduced, a locally optimal blending function is constructed purely based on the grid. A dynamic version of Vreman's sub-grid scale model (Vreman 2004; You & Moin 2007) is used to account for the physical effects of the unresolved turbulence on the resolved flow.

Two sets of simulations were conducted. One set of simulations had a spanwise domain size of 0.16 chord lengths and another had a domain size of 0.12 chord lengths. Based on *a posteriori* estimates, these spanwise domain sizes would correspond to approximately 6.7 and 5 times the boundary layer thickness (based on δ^* near the trailing

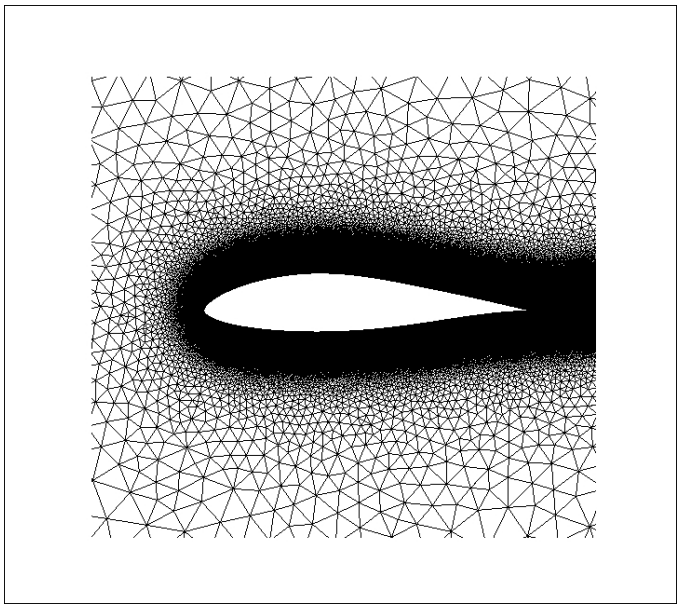

FIGURE 1. Hybrid grid generated around the DU96 airfoil. Note that the grid is structured in the near field and unstructured in the far field.

edge) respectively. Periodic boundary conditions were used in the spanwise direction. All the far-field boundaries were located approximately 10 chord lengths from the airfoil surface. A hybrid grid was used to maximize the clustering of grid points around the airfoil (Figure 1). In the far-field, an unstructured grid was used to minimize the grid points needed to spatially discretize this large domain. In the near-field, a hex-dominant grid was used to adequately resolve the turbulent structures in the boundary layer and wake. The grid size for the larger spanwise domain size was approximately 286 million elements while that for the shorter spanwise domain was 349 million elements. In the terms of wall units, the grid spacing for 286 million case at the suction side transition location is $\Delta x^+ = 37$, $\Delta y^+ = 0.8$, $\Delta z^+ = 66$ while that for the 349 million case at the same location is $\Delta x^+ = 44$, $\Delta y^+ = 1.0$, $\Delta z^+ = 29$. These represent maximum values for the two grids in terms of near wall grid spacing. The computationally intensive LES calculations were performed on the IBM BlueGene at Argonne National Laboratories. Two-dimensional calculations were done first, which then served as initial condition for the three-dimensional calculation on the 286 million grid. After interpolation from the 2D solution, the 3D calculation was run for approximately 3.6 chord flow through times. Statistics were collected over the last 1.0 time unit. Initial conditions for the 349 million grid calculation came from the 286 million grid calculation. As of writing this report, this calculation has run approximately 0.9 chord flow through times since interpolation. The solution on this grid has not yet reached a statistically steady state. Initial results obtained on this grid will be presented, primarily to draw comparisons with the 286 million grid LES.

3. Results

Figure 2 shows the pressure coefficient distribution for the 286 million grid case. Also shown in the figure are results obtained using RFOIL and XFOIL (panel codes with

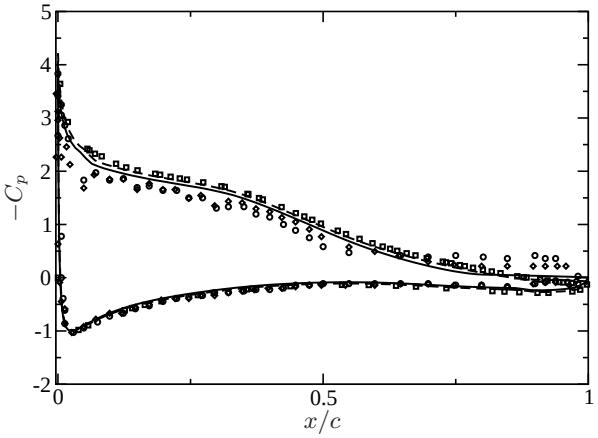

FIGURE 2. Pressure coefficient, $C_p = \frac{p-p_\infty}{\frac{1}{2}\rho_\infty U_\infty^2}$, distribution on the airfoil surface for the 286 million grid LES (□) compared against RFOIL (———) and XFOIL (- - - -) predictions as well as experimental results obtained at Virginia Tech. (Devenport *et al.* 2008). Experimental results shown are for an angle of attack of 10.3° and Reynolds numbers of 1.53×10^6 (○) and 2.85×10^6 (◇).

boundary layer corrections) and the experimental data obtained at Virginia Tech. (Devenport *et al.* 2008). LES agrees very well with XFOIL, but the agreement with experiment and RFOIL is poor, especially on the suction side of the airfoil. Over most of the suction surface, up to about $x/c = 0.7$, both LES and XFOIL are predicting lower pressures than the experiment and RFOIL. Beyond $x/c = 0.7$, the suction side pressure is almost flat in the experiment. This is generally indicative of flow separation. RFOIL also seems to be predicting trailing edge separation for this angle of attack, with the skin friction coefficient becoming negative beyond $x/c = 0.8$ (see Figure 4).

It is possible that the suction side boundary layer near the trailing edge has greater momentum in the LES than in the experiment and this might be the reason for flow separation being absent in LES. This is confirmed by the evolution of displacement and momentum thickness on the suction side (Figure 3) where LES is seen to under predict these quantities compared to RFOIL. Unfortunately, experimental data on boundary layer thickness is not available at the angle of attack studied in this report.

One possible reason for increased momentum near the trailing edge might be the transition location. Figure 4(a) shows the skin friction coefficient distribution for the 286 million grid case. Also shown in the figure are results obtained using RFOIL. Once again, experimental results on transition location or skin friction coefficient distribution were not available. The plot shows that compared to RFOIL, suction side transition is delayed in LES ($x/c = 0.09$ in RFOIL versus 0.13 in LES) while the pressure side transition happens earlier. Also, the suction side skin friction peak is under predicted by LES. This is clearly due to poor spanwise resolution in the 286 million grid LES ($\Delta z^+ = 66$) and was our main motivation for undertaking the 349 million grid LES. We also wanted to see if the improved spanwise resolution affects the transition location on both sides. Figure 4(b) shows preliminary results from the 349 million grid LES for the skin friction distribution. The improved spanwise resolution has definitely improved the skin friction peak, but the suction side transition still seems to be delayed. The prediction of boundary

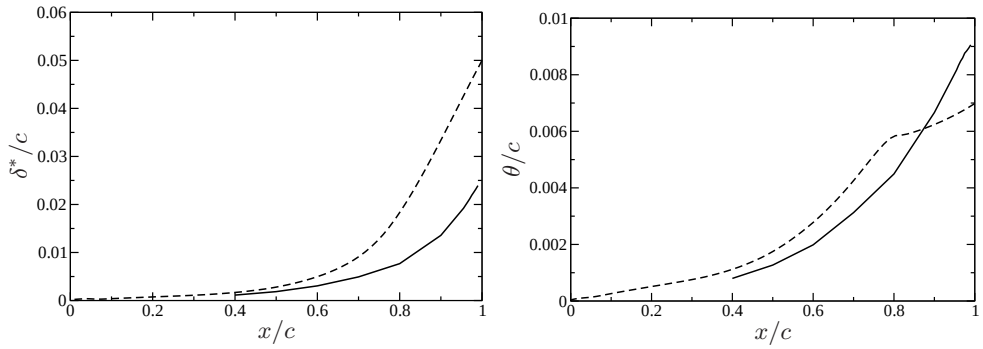

FIGURE 3. Evolution of (a) displacement and (b) momentum thicknesses for the suction side boundary layer for the 286 million grid LES. RFOIL prediction (- - - -), LES (———).

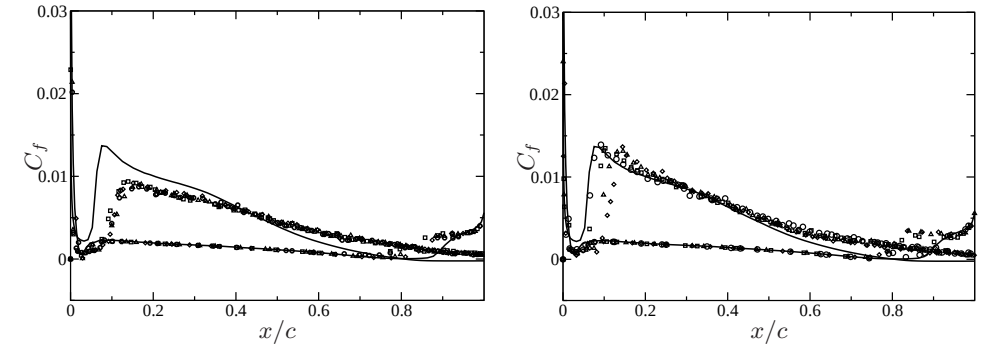

FIGURE 4. Skin friction coefficient, $C_f = \frac{\tau_w}{\frac{1}{2}\rho_\infty U_\infty^2}$, distribution for the 286 million grid LES (a) and the 349 million grid LES (b) compared against RFOIL predictions (———). In (a) the symbols represent spanwise averaged values for C_f at the following time instances: $\frac{tU_\infty}{c} = 15.35$ (○); $\frac{tU_\infty}{c} = 15.83$ (□); $\frac{tU_\infty}{c} = 16.13$ (△); $\frac{tU_\infty}{c} = 16.42$ (◇). In (b) the symbols represent the following time instances: $\frac{tU_\infty}{c} = 16.58$ (○); $\frac{tU_\infty}{c} = 16.75$ (□); $\frac{tU_\infty}{c} = 16.91$ (△); $\frac{tU_\infty}{c} = 17.08$ (◇).

layer thickness also has improved. It can be seen from Figure 5 that with advancement in time, both the momentum and displacement thickness have become closer to RFOIL predictions over $0.4 \leq x/c \leq 0.6$. Similar behavior is also noted for the suction side shape factor distribution (Figure 6).

Since the prediction of boundary layer thickness improved with spanwise resolution, we decided to assess the contribution from the subgrid stress terms. Figure 7(a) shows the ratio of subgrid to molecular viscosity. At $x/c = 0.4$, the subgrid viscosity is a non-negligible portion of the fluid viscosity near the wall. However, as we move towards the suction side trailing edge, the ratio near the wall gradually gets smaller. High values found for this ratio around $y^+ = 10^4$ occur far outside the boundary layer in the unstructured grid domain (Figure 7(b)). Another way to assess the magnitude of the subgrid stress terms is to examine the subgrid contribution to resolved scale Reynolds stress (Figure 8).

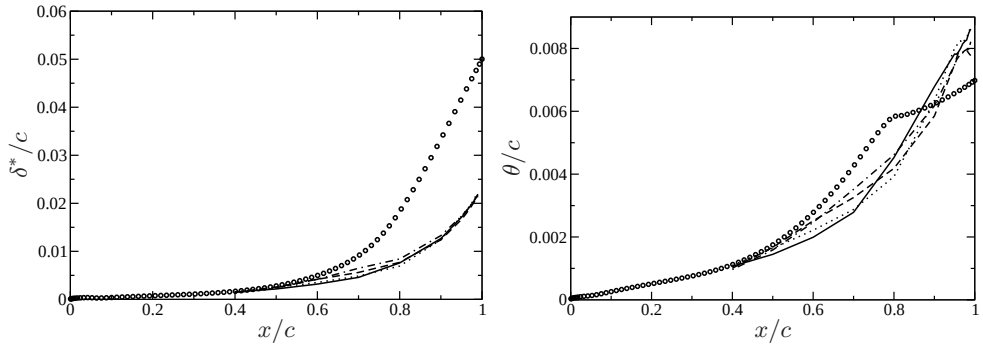

(a) (b)

FIGURE 5. Evolution of displacement (a) and momentum (b) thickness for the suction side boundary layer for the 349 million grid LES compared against RFOIL predictions (○). The lines are LES results and represent the following time instances, $\frac{tU_\infty}{c} = 16.58$ (———), $\frac{tU_\infty}{c} = 16.75$ (· · · · · · ·), $\frac{tU_\infty}{c} = 16.91$ (– – – –), $\frac{tU_\infty}{c} = 17.08$ (– · – · –).

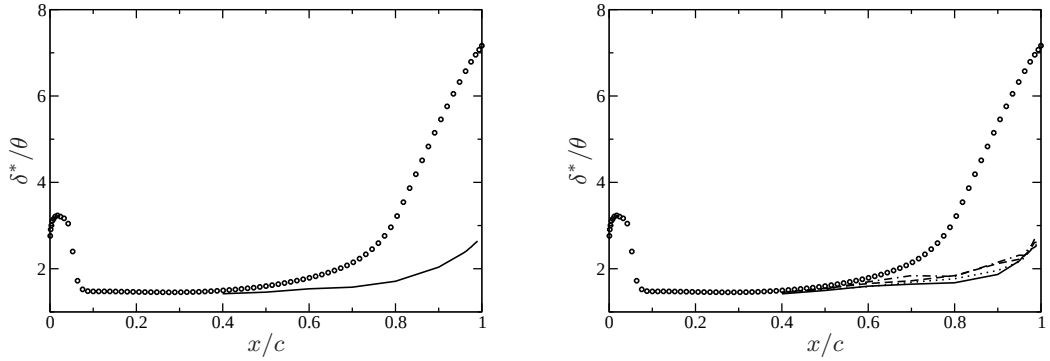

(a) (b)

FIGURE 6. Suction side shape factor for (a) the 286 million grid LES and (b) the 349 million grid LES compared against RFOIL (○). The solid lines in (b) are LES results and represent the following time instances, $\frac{tU_\infty}{c} = 16.58$ (———), $\frac{tU_\infty}{c} = 16.75$ (· · · · · · ·), $\frac{tU_\infty}{c} = 16.91$ (– – – –), $\frac{tU_\infty}{c} = 17.08$ (– · – · –).

Consistent with what was found before, at $x/c = 0.4$, the subgrid contribution is substantial in the viscous sub-layer and buffer layer while it is insignificant relative to the resolved scale Reynolds stress at $x/c = 0.9$.

Finally, a note on the experimental angle of attack quoted in Figure 2. It is an "effective" angle of attack and not the true geometric angle of attack. The difference arises due to leakage flows through the kevlar acoustic windows mounted on either side of the test section walls. The result is that the pressure distribution obtained at a particular geometric angle of attack does not match panel method predictions at the same angle of attack. However, it was found that the distributions do match, if the panel method is run at a lower angle of attack than the experiment. This was termed the effective angle of attack. In the experiment, a correction of -22% is applied to the geometric angle to

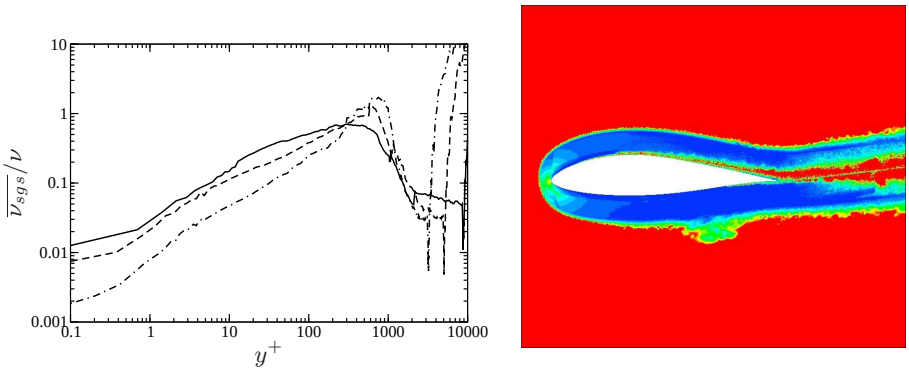

(a) (b)

FIGURE 7. Ratio of subgrid scale to molecular viscosity for the 349 million grid LES at $tU_\infty/c = 17.08$. (a) shows the spanwise average at three locations on the suction side: $x/c = 0.4$ (———), $x/c = 0.7$ (– – –), $x/c = 0.99$ (– · – · –). (b) shows contours at $z/c = 0.06$. The contours are equally spaced over the interval 0 to 1 with blue corresponding to 0 and red corresponding to 1.

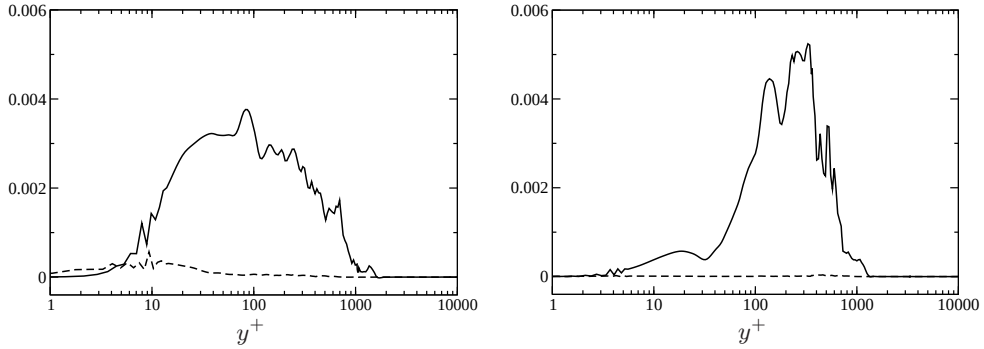

(a) (b)

FIGURE 8. Subgrid contribution to resolved scale Reynolds stress for the 349 million grid LES at $tU_\infty/c = 17.08$. Resolved scale Reynolds stress, $\overline{-u'v'}/U_\infty^2$ (———). Subgrid contribution, $\overline{\nu_{sgs}}\frac{\partial U}{\partial y}$ (– – –). (a) shows the comparison at $x/c = 0.4$ and (b) shows it as $x/c = 0.9$, both on the suction side of the airfoil.

obtain the effective angle, irrespective of the airfoil shape and the angle of attack. For example, for the effective angle quoted in Figure 2 the geometric angle of attack is 13.1°. From this discussion it is clear that there may be some uncertainty in the estimation of the effective of angle of attack. On top of this, it is noted in Devenport *et al.* (2008) that the geometric angle of attack is known only within ±0.3°. To understand whether uncertainty in the effective angle of attack can impact the indication of separation in the experiment at $\alpha = 10.2°$, we did the following test. We ran RFOIL for angles of attack of 10.0 and 10.6 degrees. This would correspond to an uncertainty of 0.3° in the chosen angle of attack of 10.3 degrees, similar to what was noted in the experiment. Results for the skin friction distribution indicate suction side separation at all three angles of attack (see Figure 9). These results indicate that the experimental uncertainty in the

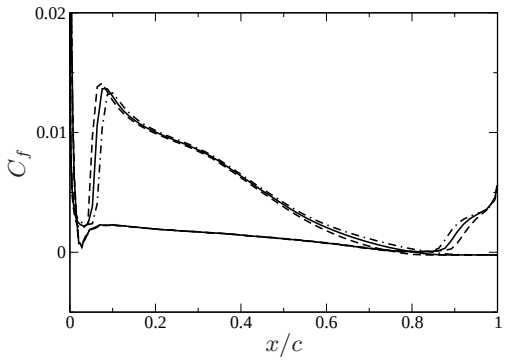

FIGURE 9. RFOIL prediction of skin friction distribution at $\alpha = 10.0^\circ$ (– · – · –), $\alpha = 10.3^\circ$ (———) and $\alpha = 10.6^\circ$ (– – – –). Suction side separation is present for all three angle of attack occurring at $x/c = 0.86$, $x/c = 0.818$ and $x/c = 0.77$ for $\alpha = 10.0^\circ$, 10.3° and 10.6° respectively.

angle of attack at 10.3 degrees may not have much impact on the presence of suction side separation at this angle.

4. Conclusions

In the present study, LES is used to simulate the airflow around the DU96 airfoil at a near stall angle of attack and at a chord-based Reynolds number of 1.5 million. Initially, an LES with 286 million elements was used to simulate the flow around the airfoil. This simulation failed to predict separation near the suction side trailing edge indicated by experimental results and RFOIL. It also predicted a thinner boundary layer near the suction side trailing edge and under predicted the skin friction peak. Subsequently, an LES with 349 million elements was attempted. Initial results from this calculation indicate that both the suction side boundary layer evolution and the prediction of skin friction peak has improved. However, further time integration of this calculation is necessary to draw definitive conclusions.

Acknowledgments

This document was prepared by GE Global Research as a result of the use of the facilities of the U.S. Department of Energy (DOE), which are managed by Brookhaven Science Associates, LLC, acting under Contract No. DE-AC02-98CH10886. Neither Brookhaven Science Associates, LLC, DOE, the U.S. Government, nor any person acting on their behalf: (a) make any warranty or representation, express or implied, with respect to the information contained in this document; or (b) assume any liabilities with respect to the use of, or damages resulting from the use of any information contained in the document. Part of this research also used resources of the Argonne Leadership Computing Facility at Argonne National Laboratory, which is supported by the Office of Science of the U.S. Department of Energy under contract DE-AC02-06CH11357.

REFERENCES

BROOKS, T. F., POPE, D. S. & MARCOLINI, M. A. 1989 Airfoil self-noise and prediction. *Tech. Rep.* 1218. NASA Reference Publication.

Christophe, J., Anthoine, J. & Moreau, S. 2009 Trailing edge noise of a controlled-diffusion airfoil at moderate and high angle of attack. *AIAA Paper 2009-3196* .

Devenport, W., Burdisso, R. A., Camargo, H., Crede, E., Remillieux, M., Rasnick, M. & Seeters, P. V. 2008 Aeroacoustic testing of wind turbine airfoils. *Tech. Rep.* 208-11-110F-101-408-1. National Renewable Energy Laboratory.

Gloerfet, X. & Garrec, T. L. 2009 Trailing edge noise from an isolated airfoil at a high reynolds number. *AIAA Paper 2009-3201* .

Khalighi, Y., Ham, F., Moin, P., Lele, S. K. & Schlinker, R. H. 2011 Scaling properties of the subgrid-scale energy dissipation in Large Eddy Simulation. In *Proceedings of the ASME Turbo Expo*.

Manoha, E., Herrero, C., Sagaut, P. & Redonnet, S. 2002 Numerical prediction of airfoil aerodynamic noise. *AIAA Paper 2002-2573* .

Moreau, S. & Roger, M. 2005 Effect of airfoil aerodynamic loading on trailing edge noise. *AIAA Journal* **43** (1).

Oberai, A., Roknaldin, F. & Hughes, T. J. R. 2002 Computation of trailing edge noise due to turbulent flow over an airfoil. *AIAA Journal* **40** (11).

Vreman, A. 2004 An eddy-viscosity subgrid scale model for turbulent shear flow: Algebraic theory and applications. *Physics of Fluids* **16**.

Wang, M. & Moin, P. 2000 Computation of trailing-edge flow and noise using large-eddy simulation. *AIAA Journal* **38** (12).

Wang, M., Moreau, S., Iaccarino, G. & Roger, M. 2004 LES predictions of pressure fluctuations on a low-speed airfoil. In *CTR Annual Research Briefs*. Center for Turbulence Research, Stanford University.

Winkler, J., Carolus, T. & Moreau, S. 2009*a* Airfoil trailing edge blowing: broadband noise prediction from large eddy simulation. *AIAA Paper 2009-3200* .

Winkler, J., Moreau, S. & Carolus, T. 2009*b* Large eddy simulation and trailing-edge noise prediction of an airfoil with boundary-layer tripping. *AIAA Paper 2009-3197* .

Wolf, W. R. & Lele, S. K. 2011 Trailing edge noise predictions using compressible les and acoustic analogy. *AIAA Paper 2011-2784* .

Wolf, W. R., Lele, S. K., Jothiprasad, G. & Cheung, L. 2012 Investigation of noise generated by a DU96 airfoil. *AIAA Paper 2012-2055* .

You, D. & Moin, P. 2007 A dynamic global coefficient subgrid scale eddy-viscosity model for large eddy simulation in complex geometries. *Physics of Fluids* **19** (6).